Comparison of Direct and Indirect Dielectric Barrier Discharge Approaches for Upscaled Production of Plasma-Activated Water

Bhagirath Ghimire[1] **and Kunning G. Xu**[2]

[1]Center for Space Plasma and Aeronomic Research, The University of Alabama in Huntsville, Huntsville, AL 35899 (USA)
[2]Department of Mechanical and Aerospace Engineering, The University of Alabama in Huntsville, Huntsville, AL 35899 (USA)

(Received: 04. January 2026, Accepted: 18. April 2026, Published online: 21. April 2026)

This study presents a comparative analysis of direct and indirect dielectric barrier discharge (DBD) approaches for the upscaled production of plasma-activated water (PAW). A cylindrical DBD reactor, consisting of nine high-voltage and nine ground electrodes operated with compressed air, was designed to investigate the generation of plasma and production of reactive oxygen and nitrogen species (RONS). The production of reactive species was evaluated through two distinct methods: indirect treatment, involving the dissolution of plasma-generated gas into water, and direct treatment, where the water flows through the active discharge region. Performance was assessed through the measurement of long-lived RONS (primarily hydrogen peroxide and nitrites), with results further analyzed through the determination of energy yields (g/kWh) and pH. The results indicate that the direct treatment approach achieves significantly higher chemical production efficiency, identifying it as the more effective strategy for the upscaled production of PAW. The relative advantages and disadvantages of both direct and indirect approaches are discussed in the context of system optimization and industrial scalability.

DOI: 10.31281/y8jmnm58

ghimirebhagi@hotmail.com

I. Introduction

Plasma activated water (PAW) has emerged as an innovative technology with the potential to contribute significantly to sustainable development [1]. PAW is formed by treating water with an ionized gas, which activates water molecules to generate highly reactive species that can be used in a wide range of applications including medicine, water treatment, agriculture, wastewater treatment, and food processing [2, 3, 4, 5, 6]. One of the key advantages of PAW is that it is an environmentally-friendly alternative to conventional chemical treatments and processes. One such example is the Haber-Bosch process, which is used to produce synthetic fertilizers. This process involves high-energy consumption and results in significant greenhouse gas emissions and has a devastating impact on the environment [7, 8]. In contrast, PAW can be generated using green technology and poses less of a burden on the environment. It has immense potential to replace traditional methods of chemical treatments and promote the health and well-being of human beings.

The reason behind the significant interest in PAW in several applications is ascribed to the production of numerous reactive oxygen and nitrogen species (RONS) such as hydrogen peroxide (H_2O_2), nitrites (NO_2^-), nitrates (NO_3^-), nitric acid (HNO_3), etc. These species are formed through the interaction of plasma components (such as electrons, ions, and UVs) with ambient gas and water molecules [2, 9, 10]. Furthermore, the chemistry of PAW including the pH can be specifically tailored by altering the feed gases and inclusion of reactive metals inside the liquid solution [11]. This makes PAW more attractive for use in several biomedical and agricultural applications.

The use of atmospheric pressure plasma sources for the production of PAW has been extensively investigated. However, the vast majority of these studies have been performed on very small liquid volumes (typically a few hundred microliters to a few milliliters) to explore the effects of operating parameters such as applied voltage, frequency and gas flow [2, 9, 12, 13]. While these laboratory-scale experiments have provided valuable mechanistic insights, they are inherently difficult to translate to industrial-scale throughputs required for practical applications in agriculture, wastewater treatment and food safety.

Although microbubble-enhanced cold plasma activation has been proposed as one promising route to improve gas-liquid mass transfer in flowing-water [14, 15, 16], this approach relies on complex Venturi injectors that can suffer from bubble coalescence, pressure drop, and long-term clogging, and still lacks systematic energy-yield benchmarking at larger scales. Critically, there remains a notable absence of comparative studies that directly evaluate direct (plasma in immediate contact with liquid) versus indirect (plasma-activated gas dissolved into liquid) treatment modes within the same upscaled reactor geometry. Such a head-to-head comparison is essential because direct interaction is expected to generate higher concentrations of reactive oxygen and nitrogen species (RONS) as a result of enhanced short-lived radical formation at the gas-liquid interface, while indirect treatment offers simpler operation but lower overall efficiency. Without this direct comparison, it is unclear which approach provides the optimal balance of RONS yield, energy efficiency, and operational simplicity for cost-effective, large-volume PAW production using inexpensive compressed air and portable power supplies.

In this article, we address this research gap by presenting a systematic comparison of direct and indirect dielectric barrier discharge (DBD) approaches for upscaled PAW production using a custom cylindrical reactor with eighteen stainless-steel electrodes.

II. Experimental Setup and Methodology

The schematic and the cross-sectional view of the reactor used for generating PAW is shown in Fig. 1a and 1b respectively. The cylindrical DBD reactor consists of eighteen stainless-steel wire electrodes (outer diameter, OD = 0.9 mm), each inserted inside individual quartz tubes (inner diameter, ID = 1 mm and OD = 2 mm). All these tubes are arranged inside a larger quartz tube(ID = 10 mm, OD = 12 mm) to generate plasma within a length of 15 cm. Nine quartz tubes containing stainless-steel wires are inserted from the top side of the quartz tube and the remaining nine quartz tubes are inserted from the bottom side following the schematic in Fig. 1b. About a 3 cm length of the stainless-steel wire remained outside of the smaller quartz tube in order to connect them to the high voltage (HV) and ground electrodes. The stainless-steel electrodes enclosed within quartz tubes remained physically isolated from both the plasma-treated water and the gas–liquid interface. As quartz is chemically inert and acts as a dielectric barrier, direct contact between the electrodes and the acidic plasma-activated water is prevented, minimizing the possibility of metal ion contamination in the activated water. A 3D-printed ceramic cap was inserted on the top and bottom end of the larger quartz tube and sealed with Torr-seal epoxy to hold the smaller quartz tubes in place and to seal the wires inside their individual small quartz tubes to prevent direct contact between the water and the metal wire electrodes. The ceramic caps also had provisions for inserting two silicone tubes (OD = 6mm) for inputting the air or water inside the reactor through one end, and outputting the plasma activated air or water through the other end. Generation of plasma was done by applying sinusoidal voltage using a commerical power supply (PVM-500, Information Unlimited, USA) between

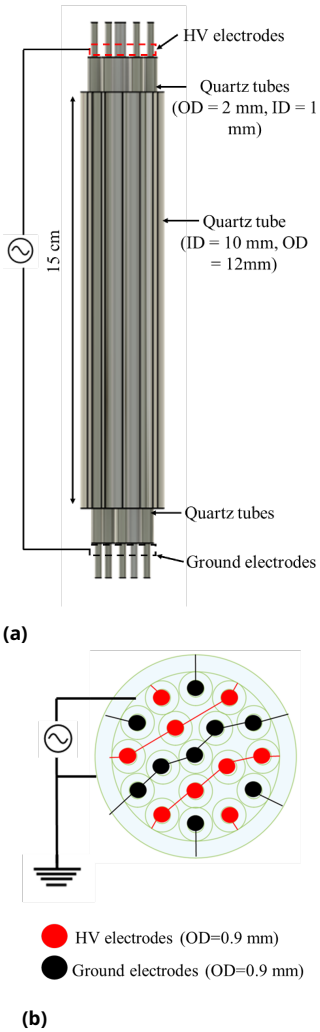

Figure 1: Schematic of: (a) the DBD reactor used to generate PAW; and (b) the arrangement of eighteen electrodes within the DBD reactor.

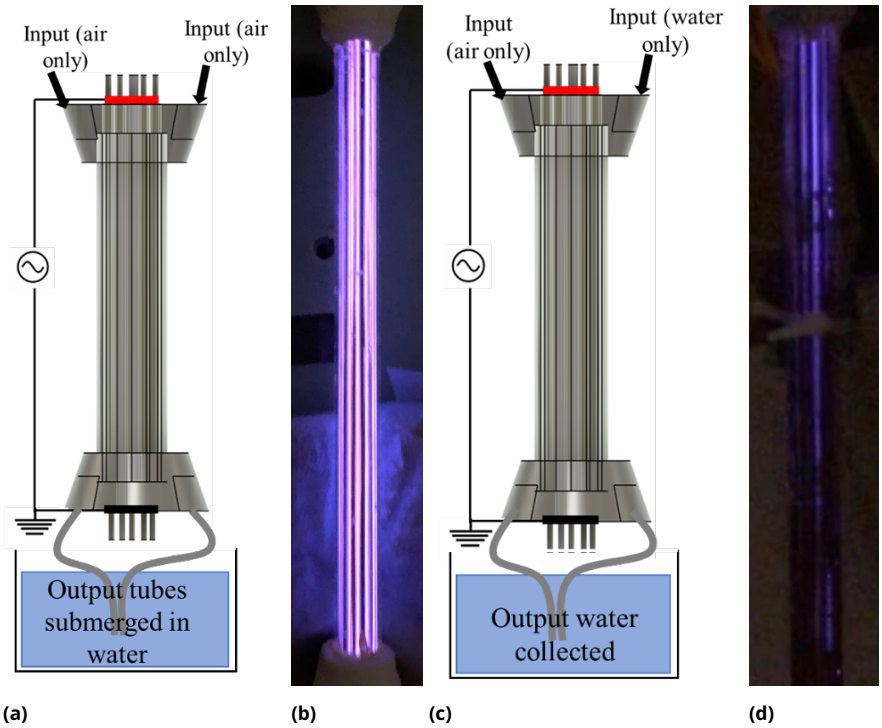

Figure 2: Methods of generating PAW through: (a) indirect (plasma-activated gas dissolved into liquid), and (c) direct (plasma in immediate contact with liquid) methods. Photographs of the discharge during operation for: (b) indirect, and (d) direct modes are also shown.

the HV and the ground electrodes. The liquid used was distilled water (conductivity: $\approx 3\ \mu S.cm^{-1}$).

The formation of RONS in PAW was investigated using two methods. In the first method (Fig. 2a), compressed air at a flow rate of 20 standard liters per minute (SLPM) was passed into the reactor through the two inlet tubes. The applied voltage was fixed at $\approx\ 10\ kV$ at $\approx\ 33\ kHz$. Under these conditions, a uniform glow discharge was formed between the HV and the ground electrodes to generate RONS from the air (Fig. 2b). The outlet tubes on the bottom side of the reactor were submerged inside a conical tube that contained fixed volume (25 mL) of water. In this configuration, RONS formed in the discharge region were carried by the gas flow and dissolved inside water, thus activating it indirectly. The indirect activation of water within a fixed volume was conducted for 5, 10, 20 and 30 minutes, and the characteristics of PAW were analyzed. In the second method (Fig. 2c), one inlet tube carried compressed air (flow rate: 50 SLPM), and the other inlet carried water into the reactor. The flow of water inside the reactor was continuous (flow rate: ≈ 25 mL/min). As water was also flowing inside the reactor, the higher flow rate of air created water bubbles inside the reactor, thus facilitating the formation of plasma. However, the plasma formed with the air and water flow from the inlet tubes Fig. 2d was very different from the one with only air flow as seen in Fig. 2b. Capturing the plasma inside individual bubbles was challenging because the discharge points continuously shift as the bubbles move and evolve. The discharge forms bright filaments or glow regions within the bubbles, which are transient and dynamically distributed during operation. In this configuration, water was directly activated within the reactor, and the activated water was collected from the outlet tubes at the bottom of the reactor. The direct activation of water with continuous flow was also conducted for 5, 10, 20 and 30 minutes, and characteristics of PAW were analyzed.

Different gas flow rates were used for the indirect and direct treatment configurations due to operational constraints related to plasma stability and species collection. In the indirect treatment mode, a flow rate of 20 SLPM was used to allow sufficient residence time and efficient dissolution of plasma-generated reactive species into water during the collection process. In the direct treatment mode, where water flows through the reactor, a higher gas flow rate of 50 SLPM was required to sustain a stable gas-phase discharge and prevent plasma quenching by the liquid medium. These flow rates represent the operational conditions necessary for stable discharge and reliable data

collection within the current reactor geometry. To ensure a meaningful comparison between the two treatment modes, the measured concentrations of reactive species were normalized as described in the Results section.

Electrical signals of the discharge were acquired by connecting a Tektronix voltage probe (Model no. P6015) to the HV tungsten electrode and a Pearson current probe (Model no. 2100) to the ground electrode. The signals from the voltage and current probes were recorded in an oscilloscope (Tektronix MDO3024). Optical emission spectroscopy of the discharge was conducted using a 0.5-m Princeton Instruments' SP2500 spectrometer coupled to a PI-MAX 4 1024×256 pixel intensified charged coupled device (ICCD) camera. The spectrometer was calibrated in wavelength and intensity using the manufacturer provided calibration lamps (Intellical, Princeton Instruments).

The chemistry of PAW after direct and indirect plasma treatment was analyzed by measuring the concentration of long-lived RONS (H_2O_2 and NO_2^-) and pH. For H_2O_2 measurements, a calibration curve with known concentrations of H_2O_2 was constructed (see Fig. A1 in the appendix) by using a colorimetric assay based on o-phenylenediamine (OPD, CAS number: 95-54-5, Sigma Aldrich Corporation) and horseradish peroxidase (HRP, CAS number: 9003-99-0, Sigma Aldrich Corporation). HRP catalyses the oxidation of OPD in the presence of H_2O_2 to form 2,3-diaminophenazine which has an absorbance maximum at 450 nm (measured using SpectraMax iD5, Molecular Devices). The line of best fit obtained from the calibration curve was then used to calculate the concentration of H_2O_2 in PAW[12, 13].

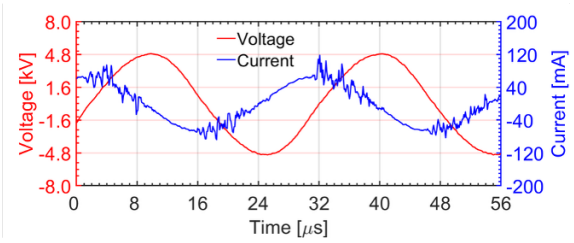

(a)

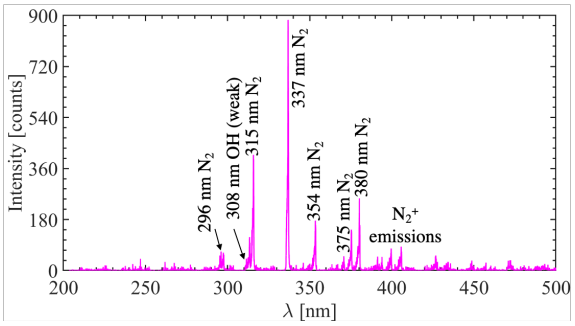

(b)

Figure 3: (a) Electrical and (b) Optical emission characteristics of the discharge recorded during indirect treatment of water with the cylindrical DBD.

Measurement of NO_2^- in PAW also involved constructing a calibration curve with known concentrations of nitrite with the help of a commercially available kit [12]. We used a Griess reagent kit (Supplier: Sigma Aldrich, EC number: 215-981-2) that gives an absorbance maximum of 540 nm (measured using SpectraMax iD5, Molecular Devices) upon reaction with the nitrites. The calibration curve constructed with known concentrations of $NaNO_2$ is shown in Fig. A2 (appendix). The line of best fit obtained from the calibration curve was then used to calculate the concentration of NO_2^- in PAW formed through indirect and direct plasma treatments.

Measurement of pH involved immersing a pH indicator paper (catalogue number: 110962, Merck Millipore) in PAW (Volume = 100 μl) and referencing the change in color, as seen with the naked eye, to the corresponding pH value on the chart provided in the kit.

III. Results and Discussion

Fig. 3 shows the electrical and optical emission characteristics of the discharge. Operation of the cylindrical DBD is done using a sinusoidal power supply with an applied voltage of ≈ 10 kV (p-p), rms current ≈35mA, frequency ≈ $33\ kHz$. The current(I) and voltage (V) waveforms of the discharge for the cylindrical DBD operating with air flow is shown in Fig. 3a. The IV-waveforms over one time period (T) were used to calculate the dissipated power (P) as:

$$P = \frac{1}{T}\int_{t=0}^{t=T} I(t)V(t)dt \qquad (1)$$

The dissipated power calculated using Eqn. (1) was 18.26 W and 22.63 W for the indirect and direct treatment methods, respectively.

Optical emission spectrum of the discharge recorded using a 0.5-m Princeton Instruments' SP2500 spectrometer coupled to a PI-MAX 4 1024×256 pixel intensified charged coupled device (ICCD) camera is shown in Fig. 3b. The spectra were recorded during indirect preparation of PAW (Fig. 2a). Several bands of nitrogen second positive system (N_2 SPS) formed through the dissociation of molecular nitrogen at 296 nm, 315 nm, 337 nm,

354 nm, 375 nm, 380 nm, 394 nm, etc. are clearly observed [17, 18, 19, 20]. Emissions from nitrogen first negative system (N_2 FNS) are also observed around 391 nm. In addition to excited nitrogen species, there is also weak emission from hydroxyl radical ($^{\bullet}$OH) at 308 nm [21, 22]. Excited nitrogen and $^{\bullet}$OH are primary species which are responsible for the formation of long-lived RONS in PAW. The measurement of hydrogen peroxide (H_2O_2) and nitrites (NO_2^-) will be described in the next paragraphs. While OES was not recorded during direct plasma treatment due to temporal and spatial instability caused by dynamic bubble formation, the discharge characteristics in this mode are expected to differ from those observed in the gas-phase configuration. In the direct treatment mode, plasma is generated within gas bubbles surrounded by liquid water, where interactions with a moisture-saturated environment and the gas–liquid interface may enhance the formation of hydroxyl radicals and other hydrogen-related reactive species compared to the indirect mode [23].

For the indirect method, the emission from N_2 SPS between 370 - 380 nm was also used to estimate the rotational and vibrational temperature of the DBD discharge using MASSIVEOES [24, 25, 26]. At atmospheric pressure, because of the high collision frequency, the gas temperature of the plasmas is close to rotational temperature. The rotational and vibrational temperature of the discharge were found to be ≈433 K and 3422 K respectively (Fig. A3, appendix). We did not record the OES of the discharge during direct plasma treatment of the flowing water (Fig. 2b), as the regions of plasma formation changed frequently with time due to bubble formation. But, due to the continuous flow of the water, the temperature of the external quartz tube was at room temperature and was monitored with a thermocouple. The temperature of the PAW collected through direct plasma treatment also remained at room temperature.

Fig. 4 shows the results for H_2O_2 concentrations in PAW. In the indirect method, the concentration of H_2O_2 increased with the treatment time up to 30 minutes. After 5 minutes, the concentration of H_2O_2 is ≈62 μM. This increased to ≈220 μM when the plasma exposure time was increased to 30 minutes. On the other hand, the concentration of H_2O_2 formed through direct method kept on decreasing. At 5 minutes, ≈305 μM of H_2O_2 was formed in PAW. This decreased by almost half (≈160 μM) when the plasma exposure time was increased to 30 minutes.

The measurements of NO_2^- concentrations for the indirect and direct methods inside PAW are shown in Fig. 5. Although, there are several nitrogen derivatives such as nitrates, nitric acid, peroxynitrous acid, etc. formed inside PAW, we measured NO_2^- to get an overall indication of reactive nitrogen species formed inside PAW. At pH values close to neutral, NO_2^- is known to be a dominant detectable species before full disproportionation into NO_3^- [27]. The concentrations of NO_2^- measured for indirectly and directly treat water are shown in Fig. 5. The trend in the NO_2^- concentrations are similar to those of H_2O_2 concentrations for both methods. For indirect method, the concentration of NO_2^- increased from ≈19 μM to ≈130 μM when the plasma exposure time was increased from 5 minutes to 30 minutes respectively. For the direct method, these concentrations decreased from ≈51 μM to ≈8 μM when the plasma treatment time increased from 5 minutes

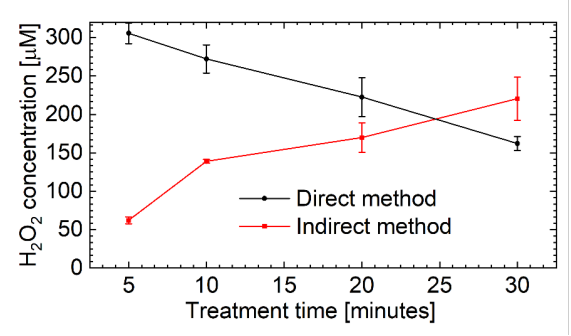

Figure 4: Concentrations of H_2O_2 measured at plasma exposure time of 5, 10, 20 and 30 minutes with the direct and indirect methods. The calibration curve used for this measurement is in the appendix (Fig. A1)

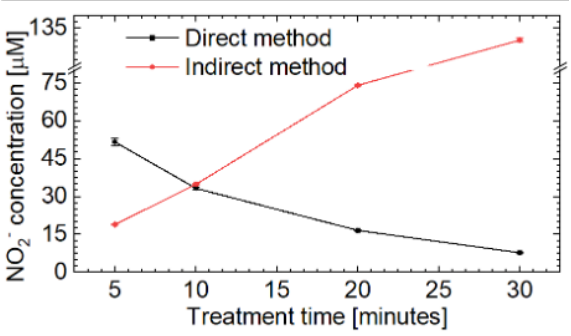

Figure 5: Concentrations of NO_2^- measured at plasma exposure time of 5, 10, 20 and 30 minutes with the direct and indirect methods. The calibration curve used for this measurement is in the appendix (Fig. A2)

to 30 minutes respectively.

The decrease in the concentrations of H_2O_2 and NO_2^- for water activated through direct method at different treatment times in Fig. 4, 5 are very interesting. It should be noted that the volume of the plasma activated water coming from the outlet tubes at different treatment times increased with time as the water was constantly pumped inside the reactor by the motor through the inlet tubes. After 5 minutes, $\approx$ 113 mL was collected in the container. This increased to $\approx$ 700 mL after 30 minutes of plasma treatment. During water flow, the formation of plasma inside the reactor only takes place inside the air bubbles. The plasma in this case is not formed at all points (as also depicted from the photograph in Fig. 2d). The formation of plasma at only few positions inside the reactor suggests that all water passing inside the reactor is not activated by the DBD plasma. We speculate that the volume of water not activated by plasma increased with time and this led to the decrease in the concentrations of H_2O_2 and NO_2^-. On the other hand, for the indirect treatment - the volume of water in the container was 25 mL and this became more concentrated when the outlet tubes were continuously submerged inside the water. This lead to the higher concentration of both H_2O_2 and NO_2^- in the plasma activated water.

To further understand the efficacy of RONS production inside PAW by the indirect and direct methods, we normalized the concentrations of H_2O_2 and NO_2^- obtained through indirect method with the total volume of water that was collected through direct method. The normalized concentration (N) for indirect plasma treatment were calculated to account for the concentration of H_2O_2 and NO_2^- that could have been formed in a total volume of collected water using direct treatment V_1 using known parameters (concentration (C_1) and volume (V_1)) for the indirect plasma treatment. This was calculated using eqn. (2) as:

$$N[\mu m] = C_1[\mu m] \times \frac{V_1[mL]}{V_2[mL]} \tag{2}$$

This normalization assumes that the total mass of RONS generated by the plasma under similar discharge conditions is conserved and that the observed concentration difference arises primarily from dilution in different liquid volumes. In practice, gas-liquid mass transfer and dissolution efficiency may also influence the measured concentrations, and therefore the normalized values should be interpreted as an approximate comparison between the two treatment modes. The results of normalization are shown in Fig. 6a,

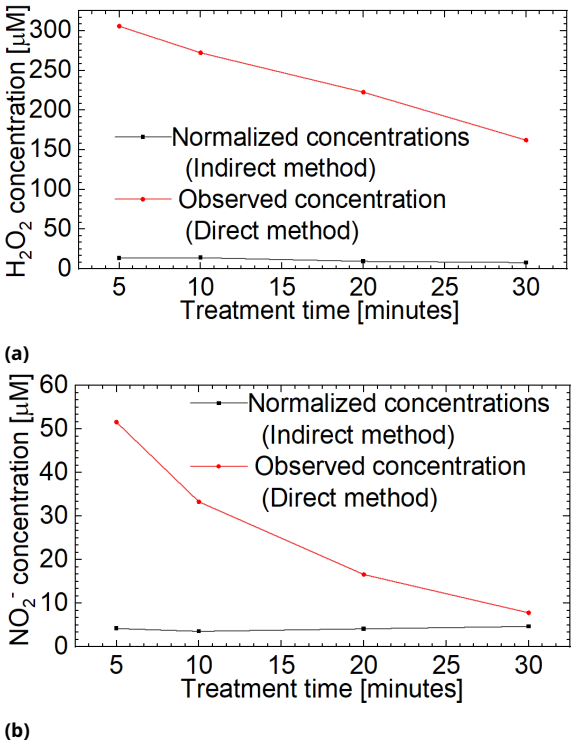

Figure 6: Normalized and observed concentrations of (a) H_2O_2 and (b) NO_2^- from indirectly and directly treated water at different plasma treatment times. The normalized values represent the concentration of H_2O_2 and NO_2^- that could have been formed when the volume of the treated water with the indirect DBD was the same as the volume of activated water collected through direct plasma treatment.

6b, and also summarized in the table (see table 1, 2 in the Appendix). Although the concentrations of both H_2O_2 and NO_2^- decreased with plasma exposure time during the direct plasma treatment, these were much higher than the normalized concentrations that could be obtained using indirect method in the same volume of target liquid. This suggests that direct treatment of water with the cylindrical DBD could be a better choice for making PAW.

We also evaluated the efficiency of direct and indirect methods by calculating the energy yield of H_2O_2 and NO_2^-. This energy yield represents the amount of chemical species generated per unit electrical energy supplied to the plasma reactor. The energy yield (EY) was calculated as:

$$EY[g/kWh] = \frac{C[mol/L].V[L].M[g/mol]}{P[kW].t[h]} \tag{3}$$

where C is the measured molar concentration in mol/L, V is the volume of treated water in L, M is the molar mass of the species in g/mol, P is

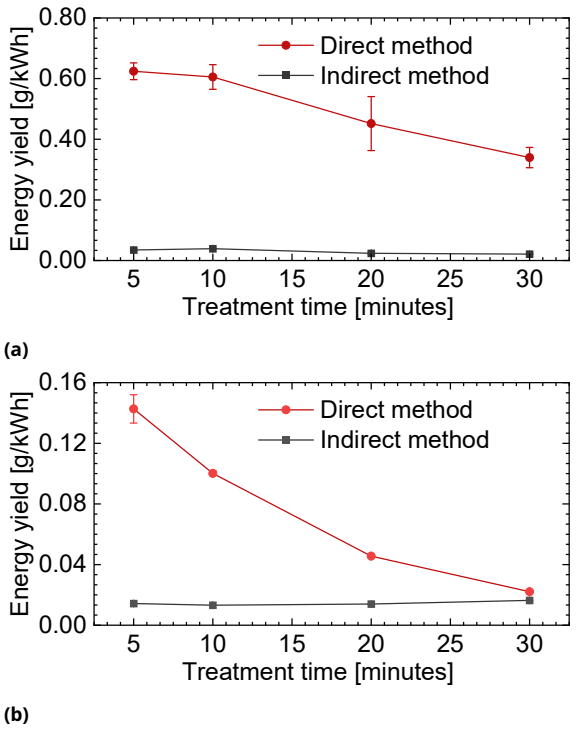

Figure 7: Estimation of energy yield for (a) H_2O_2 and (b) NO_2^- from indirect and direct treatment approaches at different plasma treatment times.

the dissipated plasma power in kW, and t is the treatment time in h. The results for 5-30 minutes of plasma treatment are presented in Fig. 7. Overall, the energy efficiency was heavily influenced by the treatment approach. The direct treatment approach [despite decrease in EY from $0.62 g/kWh$ (t=5 minutes) to $0.34 g/kWh$ (t=30 minutes)] yielded H_2O_2 concentrations approximately 16-20 times higher than those achieved via the indirect approach (Fig. 7a), identifying the direct approach as a superior strategy for the energy-efficient production of hydrogen peroxide. This enhanced efficiency is likely due to the immediate contact between the plasma and the water molecules. On the other hand, a distinct time-dependent decay in EY was observed for NO_2^- production though direct treatment approach was more efficient than the indirect one (Fig. 7b). Specifically, the EY for NO_2^- under direct treatment was ca. 10 times higher than the indirect method at t=5 minutes; however, this factor decreased to 7.60, 3.26 and 1.34 at 10, 20 and 30 minutes, respectively. The diminishing EY over time suggests that as the concentration of reactive species increase with time, secondary loss mechanisms could become more dominant.

The reason for higher concentrations of both H_2O_2 and NO_2^- in the directly activated water with the cylindrical DBD are due to the differences in the mode of activation. Formation of H_2O_2 and NO_2^- inside the DBD reactor mainly takes place through the dissociation of H_2O, O_2 or N_2 below [28, 2, 29, 19, 30, 12] :

(1) $e^- + O_2 \rightarrow O(^3P) + O(^1D) + e^-$, $O(^1D)+H_2O \rightarrow 2^\bullet OH$
(2) $e^- + N_2 \rightarrow N_2(A^3\sum_u^+) + e^-$, $N_2(A^3\sum_u^+) + H_2O \rightarrow {}^\bullet OH+N_2+{}^\bullet H$
(3) $UV + H_2O \rightarrow H_2O^*$; $UV + H_2O^* \rightarrow H^+ + OH^-$; $OH^- \rightarrow {}^\bullet OH+ e^-$
(4) $e^- + N_2 \rightarrow N + N + e^-$
(5) $e^-+O_2 \rightarrow O + O + e^-$
(6) $N+O_2 \rightarrow NO + O$;
(7) $N + {}^\bullet OH \rightarrow NO + {}^\bullet H$;
(8) $N+O \rightarrow NO$

The $^\bullet OH$ and NO so formed in (1)-(8) recombine to form H_2O_2 and NO_2^- as follows [31, 32]:

(9) $^\bullet OH + {}^\bullet OH \rightarrow H_2O_2$
(10) $4NO + 2O_2 + 2H_2O \rightarrow NO_2^- + 4H^+$

During direct plasma treatment, most of the reactions [(1)-(10)] take place within the DBD reactor where high energy electrons and excited species interact directly with the ambient gas species (H_2O, N_2, O_2). As a result, H_2O_2 and NO_2^- could be formed instantaneously within the discharge region. On the other hand, during indirect plasma treatment, it is mainly the plasma activated gas that interacts with the target liquid to result in the production of H_2O_2 and NO_2^-. Since the lifetime of short-lived reactive species (such as $^\bullet OH$, O, N, etc.) is short [32, 28], only the long-lived species formed in the discharge region are carried/dissolved onto the target water resulting in the lower concentration of both H_2O_2 and NO_2^-.

NO_2^- or HNO_2 formed in PAW can also combine with H_2O_2 to form NO_3^- or ONOOH as [12]:

(11) $NO_2^- + H_2O_2 + H^+ \rightarrow NO_3^- + H_2O + H^+$
(12) $HNO_2 + H_2O_2 \rightarrow ONOOH + H_2O$

Although, the concentration of NO_3^- was not explicitly measured in this work, the simultaneous decrease in EY of both H_2O_2 and NO_2^- (Fig. 7) suggests that reactions (11)-(12) could be responsible for the secondary loss.

The final set experiments were designed to investigate the effect of plasma treated solutions (indirect and direct) on pH. pH is an important parameter that affects the growth of plants [33]. The level of pH plants require for growth may be different but most of the plants prefer to grow

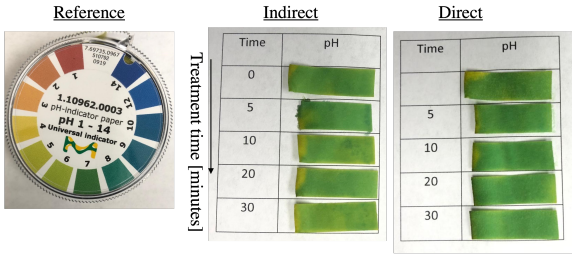

Figure 8: pH of PAW prepared through indirect and direct treatment of water.

around neutral pH. The pH of PAW normally goes to acidic level upon exposure to plasma treatment. For example, the pH of 5 minutes PAW prepared with plasma jet is between 2-3 [12]. In this work, a pH indicator paper was primarily used to provide a visual confirmation of the pH change in plasma-activated water. Although this method provides only semi-quantitative estimation, it effectively illustrates the relative pH difference between untreated and plasma-treated samples. Despite activating for up to 30 minutes, the pH of PAW prepared at different treatment times with both indirect and direct methods remained close to neutral (Fig. 8) and this could favor the growth of several plants.

IV. Conclusions

In conclusion, a comparison on the characteristics of PAW prepared through indirect and direct activation of water by a cylindrical atmospheric pressure DBD reactor operated with compressed air is presented in this work. The DBD operated with only air flow runs at higher gas temperature leading to heating of the DBD reactor. On the other hand, the flow of liquid inside the DBD reactor results in the lower heating of the reactor but formation of plasma is not uniform. Results obtained from the chemical analysis of PAW suggest that concentration of H_2O_2, NO_2^- (and other RONS that could be present inside PAW) are higher from directly activated PAW which were verified through the normalization experiments and calculation of energy efficiencies. The pH of the PAW prepared using both methods remained close to neutral. The approach presented in this study could be scaled towards production of PAW in large quantities for applications in agriculture and medicine.

V. Acknowledgement

This work was supported by NSF EPSCoR RII-Track-1 Cooperative Agreement OIA-2148653.

VI. References

[1] Kiing S. Wong,Nicholas S.L. Chew, Mary Low and Ming K. Tan, "Plasma-Activated Water: Physicochemical Properties, Generation Techniques, and Applications," *Processes (MDPI)*, vol. 11, p. 2023, 2023.

[2] N. K. Kaushik, B. Ghimire, Y. Li, M. Adhikari, M. Veerana, et al., "Biological and medical applications of plasma-activated media, water and solutions," *Biological Chemistry*, vol. 400, p. 39, 2019.

[3] R. P. Gott, M. E. Thompson, B. C. Staton, B. M. Williams and K. G. Xu, "Analysis of Time-Resolved Plasma Jet Emissions That Drive Methylene Blue Dye Decomposition," *IEEE Transactions on Plasma Science*, vol. 49, p. 2113, 2021.

[4] Shivangi Srivastava, Ubaida Akbar, Md Sabir Ahmed Mondol, Kshirod Kumar Dash, Pir Mohammad Junaid, et al., "Plasma Activated Water in Enhancing Food Safety and Quality: A Comprehensive Review," *Plasma Chem Plasma Process*, vol. 45, p. 1603, 2025.

[5] P. Lamichhane, M. Veerana, J. S. Lim, S. Mumtaz, B. Shrestha, et al., "Low-Temperature Plasma-Assisted Nitrogen Fixation for Corn Plant Growth and Development," *International Journal of Molecular Sciences*, vol. 22, p. 5360, 2021.

[6] M. Laroussi, "Low-Temperature Plasma Jet for Biomedical Applications: A Review," *IEEE Transactions on Plasma Science*, vol. 43, p. 703, 2008.

[7] Pradeep Lamichhane, Bishwa Chandra Adhikari, Linh N Nguyen, Ramhari Paneru, Bhagirath Ghimire, et al., "Sustainable nitrogen fixation from synergistic effect of photo-electrochemical water splitting and atmospheric pressure N_2 plasma," *Plasma Sources Science and Technology*, vol. 29, p. 045026, 2020.

[8] D. Panchal, Q. Lu, K. Sakaushi, and X. Zhang, "Advanced cold plasma-assisted technology for green and sustainable ammonia synthesis," *Chemical Engineering Journal*, vol. 498, p. 154920, 2024.

[9] A. Khlyustova, C. Labay, Z. Machala, M. P. Ginebra, and C. Canal, "Important parameters in plasma jets for the production of RONS in liquids for plasma medicine: A brief review," *Frontiers of Chemical Science and Engineering*, vol. 13, p. 238, 2019.

[10] Sushil Kumar K.C., B. Ghimire, Sung-Ha Hong, Jun-Seok Oh and Endre J Szili, "How to control the plasma jet production of reactive species for medical therapy? A topical review," *Journal of Physics D: Applied Physics*, vol. 58, p. 143006, 2025.

[11] Pradeep Lamichhane, Ramhari Paneru, Linh N Nguyen, Jun Sup Lim, Pradeep Bhartiya, et al., "Plasma-assisted nitrogen fixation in water with various metals," *Reaction Chemistry Engineering*, vol. 5, p. 2053, 2020.

[12] B. Ghimire, E. J. Szili, B. L. Patenall, P. Lamichhane, N. Gaur, et al., "Enhancement of hydrogen peroxide production from an atmospheric pressure argon plasma jet and implications to the antibacterial activity of plasma activated water," *Plasma Sources Science and Technology*, vol. 30, p. 035009, 2021.

[13] B. Ghimire, B. L. Patenall, E. J. Szili, N. Gaur, P. Lamichhane, et al., "The influence of a second ground electrode on hydrogen peroxide production from an atmospheric pressure argon plasma jet and correlation to antibacterial efficacy and mammalian cell cytotoxicity," *Journal of Physics D: Applied Physics*, vol. 55, p. 125207, 2022.

[14] Z. Saedi, M. Kuddushi, Y. Gao, D. Panchal, B. Zeng, et al., "Stable and efficient microbubble-enhanced cold plasma activation for treatment of flowing water," *Sustainable Materials and Technologies*, vol. 40, p. e00887, 2024.

[15] Z. Saedi, D. Panchal, Q. Lu, M. Kuddushi, S. E. Pour, et al., "Integrating multiple cold plasma generators and Bernoulli-driven microbubble formation for large-volume plasma treatment," *Sustainable Materials and Technologies*, vol. 44, p. e01300, 2025.

[16] N. Shahsavari, and X. Zhang, "Microbubble-enhanced cold plasma activation for decontamination: Degradation dynamics and energy yield in relation to pollutant concentration, total volume and flow rate of water," *Journal of Water Process Engineering*, vol. 55, p. 104169, 2023.

[17] R. P. Gott and K. G. Xu, "OH Production and Jet Length of an Atmospheric-Pressure Plasma Jet for Soft and Biomaterial Treatment," *IEEE Transactions on Plasma Science*, vol. 47, p. 4988, 2019.

[18] E. J. Baek, H. M. Joh, S. J. Kim, and T. H. Chung, "Effects of the electrical parameters and gas flow rate on the generation of reactive species in liquids exposed to atmospheric pressure plasma jets," *Physics of Plasmas*, vol. 23, p. 073515, 2016.

[19] B. Ghimire, J. Sornsakdanuphap, Y. J. Hong, H. S. Uhm, K. D. Weltmann, et al., "The effect of the gap distance between an atmospheric-pressure plasma jet nozzle and liquid surface on OH and N2 species concentrations," *Physics of Plasmas*, vol. 18, p. 073502, 2017.

[20] B. Ghimire, P. Lamichhane, J. S. Lim, B. Min, R. Paneru, et al., "An atmospheric pressure plasma jet operated by injecting natural air," *Applied Physics Letters*, vol. 113, p. 194101, 2018.

[21] A. Sarani, A. Y. Nikiforov and C. Leys, "Atmospheric pressure plasma jet in Ar and mixtures: Optical emission spectroscopy and temperature measurements," *Physics of Plasmas*, vol. 17, p. 063504, 2010.

[22] M. Thiyagarajan, A. Sarani, and C. Nicula *Journal of Applied Physics*, vol. 113, p. 233302, 2013.

[23] P.J. Bruggeman, M. J. Kushner, B.R. Locke, J.G.E. Gardeniers, W. G. Graham, et al., "Plasma–liquid interactions: a review and roadmap," *Journal of Physics D: Applied Physics*, vol. 25, p. 053002, 2016.

[24] J. Vorac. P. Synek, L. Potocnakova, J. Hnilica and V. Kudrle, "Batch processing of overlapping molecular spectra as a tool for spatio-temporal diagnostics of power modulated microwave plasma jet," *Plasma Sources Science and Technology*, vol. 30, p. 025010, 2017.

[25] J. Vorac, P. Synek, V. Prochazka and T. Hoder, "State-by-state emission spectra fitting for non-equilibrium plasmas: OH spectra of surface barrier discharge at argon/water interface," *Journal of Physics D: Applied Physics*, vol. 50, p. 294002, 2017.

[26] J. Vorac, L. Kusyn and P. Synek, "Deducing rotational quantum-state distributions from overlapping molecular spectra," *Review of Scientific Instruments*, vol. 19, p. 123102, 2019.

[27] M. Zhang, T.Lin, G. Liu, B. Wu, X. Wang, et al., "The influence of pH value on nitrate and nitrite formation in air-plasma-treated aqueous solutions," *Plasma Science and Technology*, vol. 27, p. 095508, 2025.

[28] X. Pei, Y. Lu, S. Wu, Q. Xiong and X. Lu, "A study on the temporally and spatially resolved OH radical distribution of a room-temperature

atmospheric-pressure plasma jet by laser-induced fluorescence imaging," *Plasma Sources Sci. Technol.*, vol. 22, p. 025023, 2013.

[29] E. J. Szili, B. Ghimire, B. L. Patenall, M. Rohaim, D. Mistry, et al., "On-demand cold plasma activation of acetyl donors for bacteria and virus decontamination," *Applied Physics Letters*, vol. 119, p. 054104, 2021.

[30] B. Ghimire, E. J. Szili, P. Lamichhane, R. D. Short, J. S. Lim,et al., "The role of UV photolysis and molecular transport in the generation of reactive species in a tissue model with a cold atmospheric pressure plasma jet ," *Applied Physics Letters*, vol. 114, p. 093701, 2019.

[31] H. S. Uhm, "Generation of various radicals in nitrogen plasma and their behavior in media," *Phys. Plasmas*, vol. 22, p. 123506, 2015.

[32] P. Attri, Y. H. Kim, D. H. Park, J. H. Park, Y. J. Hong, et al., "Generation mechanism of hydroxyl radical species and its lifetime prediction during the plasma-initiated ultraviolet (UV) photolysis," *Scientific Reports*, vol. 5, p. 9332, 2015.

[33] Jong-Seok Song and Sunkyung Jung, "The pH acidity and nitrate accumulation by plasma discharge enhanced the growth and phytochemicals of soybean sprouts grown in reused water," *Food Chemistry: X*, vol. 22, p. 101345, 2024.

VII. Data Availability Statement

All data that support the findings of this study are included within the article and its appendix.

VIII. Appendix

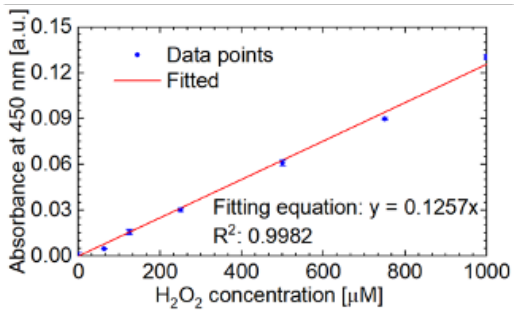

Figure A1: Calibration curve constructed with known concentrations of H_2O_2 for estimating the concentration of H_2O_2 in PAW.

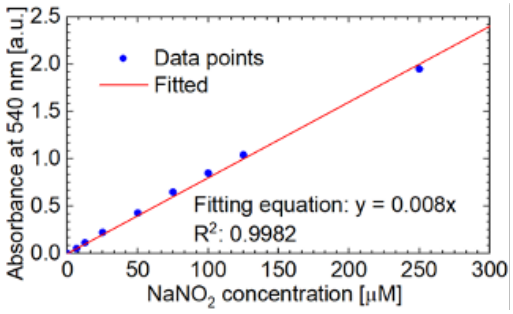

Figure A2: Calibration curve constructed with known concentrations of $NaNO_2$ for estimating the concentration of NO_2^- in PAW.

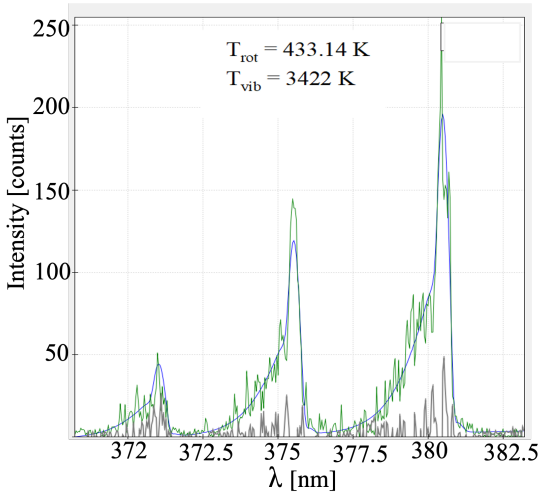

Figure A3: Measurement of rotational and vibrational temperature of the DBD discharge (for indirectly preparing PAW) using MASSIVEOES.

T [min]	C_1 [μM]	V_1 [mL)	V_2 [mL]	N [μM]
5	62.22	25	113.33	13.72
10	139.12	25	246.67	14.10
20	169.87	25	450.00	9.44
30	220.53	25	696.67	7.91

Table 1: Normalized concentrations of H_2O_2 for the indirect treatment by considering the volume of liquid collected with direct plasma treatment. The normalized values represent the concentration of H_2O_2 and NO_2^- that could have been formed when the volume of the treated water with the indirect DBD was the same as the volume of activated water collected through direct plasma treatment.

T [min]	C_1 [μM]	V_1 [mL)	V_2 [mL]	N [μM]
5	18.94	25	113.33	4.18
10	34.90	25	246.67	3.54
20	74.10	25	450.00	4.12
30	130.24	25	696.67	4.67

Table 2: Normalized concentrations of NO_2^- for the indirect treatment by considering the volume of liquid collected with direct plasma treatment. The normalized values represent the concentration of H_2O_2 and NO_2^- that could have been formed when the volume of the treated water with the indirect DBD was the same as the volume of activated water collected through direct plasma treatment.